PHYSICAL REVIEW A VOLUME 23, NUMBER 1 JANUARY 1981

High-resolution spectroscopy of molecular hydrogen in the extreme ultraviolet region

M. Rothschild, H. Egger, R. T. Hawkins,* J. Bokor,† H. Pummer, and C. K. Rhodes
Department of Physics, University of Illinois at Chicago Circle, P.O. Box 4348, Chicago, Illinois 60680
(Received 28 July 1980)

We report high-resolution spectroscopy of the $D\ ^1\Pi_u$, $D''\ ^1\Pi_u$, and $B''\ ^1\Sigma_u^+$ states in H_2, HD, and D_2, performed in absorption in the vicinity of 83 nm. Predissociative widths as narrow as 0.3 cm^{-1} have been measured, and profile analyses based on the theory of Fano are performed on these predissociated states. The importance of overlap integrals in the predissociation of B'' is shown, and the absorption cross section $\sigma = (7.2 \pm 0.7) \times 10^{-16}$ cm^2 for the $B'' \leftarrow X(2,0)$ is determined. Anomalous behavior observed in the D ($v = 5$) states of D_2 is analyzed in terms of an accidental perturbation by the D'' ($v = 0$) states.

I. INTRODUCTION

The hydrogen molecule, and in particular the structure and spectrum of its electronically excited states, has been the subject of intensive theoretical and experimental study in recent years.[1-12] The importance of the hydrogen spectrum is well known; primarily, since hydrogen is the simplest of all many-electron molecules, its spectrum is the testing ground of both refined calculations and improved experimental techniques. Furthermore, the excited states of the hydrogen molecule are of considerable relevance to chemistry and astrophysics.

Experimental studies of the excited states of the hydrogen molecule utilizing optical excitation require sources of radiation in the region 80 to 120 nm (ionization of H_2 takes place at wavelengths below 80.4 nm). Until recently, the only sources available in this spectral region have been weak, broadband incoherent sources such as a helium lamp or a synchrotron. The radiation from a synchrotron is normally dispersed with a vacuum monochromator, a procedure which establishes, at best, an instrumental resolution[2,10,11] on the order of ~2.5 cm^{-1}. This instrumental width is more than twice the Doppler width of H_2 at room temperature, and three times that of D_2. High-resolution studies of hydrogen in absorption have thus been severely limited by the unavailability of bright, narrow bandwidth sources in the extreme ultraviolet (xuv). In particular, the predissociative width of only rather broad lines (≥ 3 cm^{-1})[3,10] could be measured. Certain predissociated lines in H_2 and in HD, and most predissociated lines in D_2, could not be analyzed with this resolution.[12,13]

In this paper we report the results of high-resolution studies performed in the vicinity of 83 nm in H_2, HD, and D_2. In these studies, absorption line centers and line shapes were determined with great accuracy, enabling the analysis of the roles of both overlap integrals and accidental perturbations. These studies were made possible by the development of a bright, coherent, high-resolution source, tunable around 83 nm.[14]

Despite the apparent simplicity of the hydrogen molecule, its excited states display a variety of properties whose analysis is far from being simple. Many of these properties arise due to failure of the Born-Oppenheimer approximation: predissociation,[1-3,11-13] lambda doubling,[5,7,12,15] and irregularities in ro-vibronic line positions and intensities.[7] In general, diabatic interactions between two electronic states ξ and ξ' with total electronic angular momentum about the internuclear axis Λ and Λ', respectively, can be classified into two categories[16]: (a) Homogeneous if $\Lambda' = \Lambda$. In this case the coupling is between the vibrational and the electronic degrees of freedom and is independent of molecular rotations. (b) Heterogeneous, if $\Lambda' = \Lambda \pm 1$. This interaction couples electronic motion and molecular rotation with a coupling energy proportional (in the pure precession approximation) to[7] $J(J+1)$, where J is the rotational quantum number.

As examples, lambda doubling,[17] in which the $(np\pi)\,^1\Pi_u^{\pm}$ degeneracy is removed by $(np\pi)\,^1\Pi_u^+ - (np\sigma)\,^1\Sigma_u^+$ interaction, is a heterogeneous coupling. The $^1\Pi_u^+ - {}^1\Pi_u^-$ energy splitting is approximately proportional to[5,17] $J(J+1)$. Predissociation may be predominantly heterogeneous, as when $D(3p\pi)\,^1\Pi_u^+$ is predissociated[1,3] by $B'(3p\sigma)\,^1\Sigma_u^+$, or it may be homogeneous, as when $B''(4p\sigma)\,^1\Sigma_u^+$ is predissociated[13] by $B'(3p\sigma)\,^1\Sigma_u^+$. Other homogeneous or heterogeneous interactions are possible, some due to accidental proximity of two states.

The most strongly predissociated state in H_2 above ~14.5 eV is[1,3,11] $D(3p\pi)\,^1\Pi_u$, which interacts with the continuum of the $B'(3p\sigma)\,^1\Sigma_u^+$ state (see Fig. 1 for the relevant states). The $(np\sigma)\,^1\Sigma_u^+$ states ($n \geq 4$) are homogeneously coupled to the same continuum. The B' continuum is also responsible for the predissociation of the $(np\pi)\,^1\Pi_u$ states[2,17,18] ($n \geq 4$), this time via second-order channels[18]: (a) homogeneous $(np\pi)\,^1\Pi_u - (3p\pi)\,^1\Pi_u$, followed by hetero-

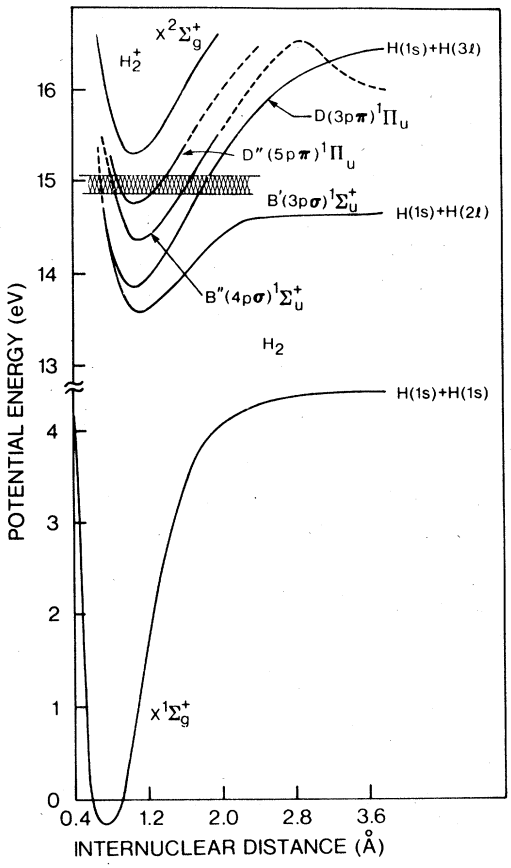

FIG. 1. The relevant states in H_2 (from Ref. 21). The shaded area is the area accessible by the 83-nm source.

geneous $(3p\pi)^1\Pi_u - (3p\sigma)^1\Sigma_u^+$ interactions. (b) Heterogeneous $(np\pi)^1\Pi_u - (np\sigma)^1\Sigma_u^+$ followed by $(np\sigma)^1\Sigma_u^+ - (3p\sigma)^1\Sigma_u^+$ interaction. As expected, the higher order predissociation yields are much lower than those of the direct first order predissociation.[1,17] Also, in the case of the $(np\pi)^1\Pi_u$ states ($n \geq 3$), the lambda-minus components are forbidden by symmetry to interact with B' $(3p\sigma)^1\Sigma_u^+$. Therefore, the $(np\pi)^1\Pi_u^-$ states do not predissociate at all,[1] except possibly very weakly through a homogeneous interaction with the continuum of the C $(2p\pi)^1\Pi_u^-$ state.[17] From symmetry considerations,[16] Q-branch transitions from the ground state excite the $^1\Pi_u^-$ states, while P- and R-branch transitions excite the $^1\Pi_u^+$ states. There is no Q branch in the $^1\Sigma_g^+ - {}^1\Sigma_u^+$ transitions.

II. EXPERIMENTAL

The experimental configuration is shown schematically in Fig. 2 and Fig. 3. In the first stage (Fig. 2), a single-frequency cw dye laser (Coherent model CR-599, ~497 nm) was amplified in a

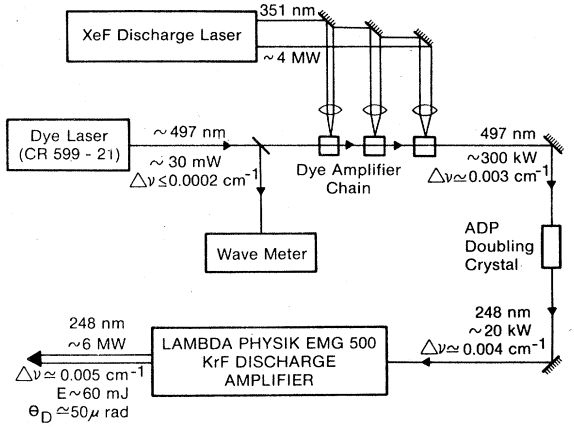

FIG. 2. The system which generates the narrow-bandwidth KrF* source (see text).

pulsed fashion. The amplifiers consisted of four dye cuvettes, pumped by a XeF* (351 nm), Lambda Physik model EMG 500, excimer laser. The amplified dye laser consisted of ~5-mJ pulses of 15 nsec full width at half maximum (FWHM), with a measured line width of 0.003 cm^{-1}. Absolute wavelength calibration was performed with the wavemeter, which monitored the cw dye laser. In the second stage[19] (Fig. 2), the blue laser was frequency-doubled in a temperature-controlled ammonium dihydrogen phosphate (ADP) crystal. This second harmonic radiation (~1 mJ at 248 nm) was amplified in a single-pass KrF* excimer amplifier (Lambda Physik model EMG 500). The output was a 60-mJ, 15 nsec pulse at 248 nm, with a measured bandwidth[19] of 150 ± 20 MHz and divergence of ~50 μrad. In the third stage[14] (Fig. 3), the 248-nm source was frequency tripled in xenon. This was accomplished by focusing it with a CaF_2 10-cm-focal-length lens into a cell containing gaseous xenon at ~10 torr. The xenon was differentially pumped through a 0.35-mm pinhole, the focal spot being located at the pinhole. The 83-nm radiation obtained in this fashion was passed

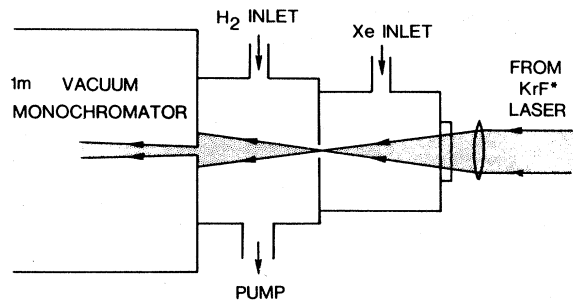

FIG. 3. The system which generates the 83-nm source (see text).

through a 1-m vacuum monochromator and detected by an electron multiplier, whose output was fed into a transient digitizer and stored in a computer. The tripling efficiency was estimated to be $\sim 10^{-10}$ over most of the tuning range, with a hundred-fold enhancement at 249.6 nm, which coincides with a two-photon resonance in xenon.

The gases used in the experiments were H_2: 99.9999% pure (Scientific Gas Products); HD: 98% pure (Merck Sharp and Dohme); and D_2: 99.99% pure (Air Products). The gas was under continuous flow; it was let into the differentially pumped chamber, and pumped out together with the xenon. A MKS Baratron (170 M) pressure gauge, located on the side of the chamber, indicated the background pressure. The hydrogen pressure in the 83-nm radiation region is expected to be spatially nonuniform and strongly dependent on the characteristics of hydrogen penetration into the xenon "plume." The experiments have shown that, at pressures above 40 mtorr in H_2 and 30 mtorr in HD, the extinction coefficient of hydrogen was proportional to the background pressure reading. Therefore, we assumed that the average hydrogen pressure in the absorption region was equal to the background pressure. Based on this assumption, the absolute cross section for the $B''\leftarrow X$ transition was calculated (see Sec. IV). The absorption curves were obtained at each frequency from the transmitted 83-nm radiation with and without hydrogen present.

III. DATA ANALYSIS AND RESULTS

Several of the observed absorption lines had symmetric profiles, whose width corresponded to the Doppler width characteristic of room temperature: 1.0 cm^{-1} in H_2, 0.84 cm^{-1} in HD, and 0.73 cm^{-1} in D_2. Other lines had asymmetric profiles which were manifestly broader than the Doppler width. The asymmetric line shapes can be understood in terms of the theory[20] developed by Fano concerning discrete state-continuum state interaction. According to that analysis, this interaction results in an interference which distorts the shape of the mixed state and shifts the center frequency relative to the position of the unperturbed discrete state.

The frequency dependence of the resultant absorption cross section $\sigma(\nu)$ is

$$\sigma(\nu) \propto \frac{\left(q + \frac{\nu - \nu_0}{\frac{1}{2}\Gamma}\right)^2}{1 + \left(\frac{\nu - \nu_0}{\frac{1}{2}\Gamma}\right)^2} \quad . \tag{1}$$

In Eq. (1), ν_0 is the (new) center frequency, Γ is the predissociative linewidth, and q is the asymmetry parameter. The quantities Γ and q are defined by

$$\Gamma \equiv 2\pi |\langle \Psi | H | \xi \rangle|^2 \, , \tag{2}$$

$$q \equiv \frac{\langle \phi | T | i \rangle}{\pi \langle \xi | H | \Psi \rangle \langle \Psi | T | i \rangle} \quad . \tag{3}$$

In Eqs. (2) and (3), H is the part of the molecular Hamiltonian which couples the discrete and the continuum states, and T is the dipole moment operator. The states are: $|i\rangle$ the initial (ground) state, $|\xi\rangle$ the discrete state, $|\Psi\rangle$ the continuum state, and $|\phi\rangle$ the "modified" discrete state. From Eq. (3), q can be either positive or negative, depending on the signs of the three matrix elements involved. Also, the larger the magnitude of q, the smaller the degree of asymmetry.

The asymmetric lines which were observed in absorption represent the convolution of the appropriate Doppler profile and a Fano profile [Eq. (1)].

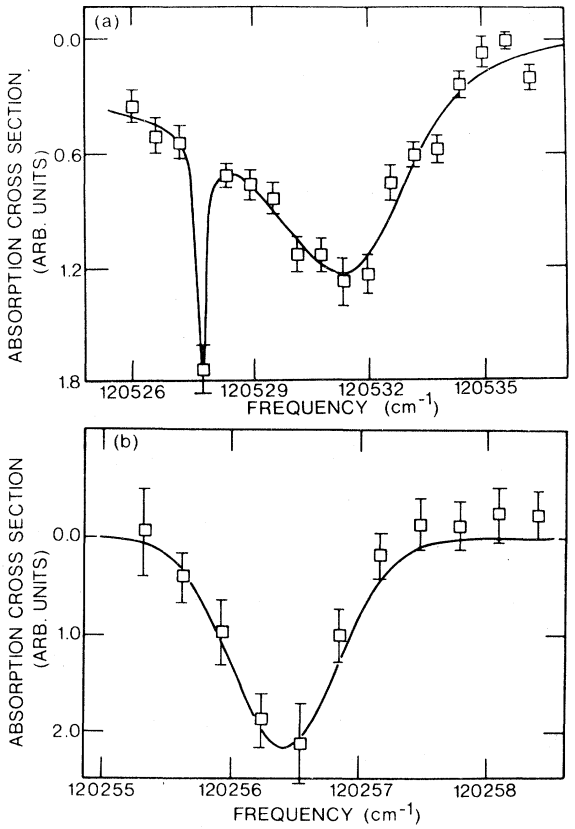

FIG. 4. Two typical absorption lines at 83 nm. (a) The broad, asymmetric $D\leftarrow X$ (5, 0) $R(2)$ transition in D_2. Superimposed on it is the narrow $D\leftarrow X$ (5, 0) $Q(1)$ line. The solid line is the best fit (see text). (b) The narrow, symmetric $D''\leftarrow X$ (0, 0) $R(1)$ transition in H_2. The solid line is a Gaussian profile with Doppler width.

The Fano profile included four as yet undetermined quantities: its overall strength, the center ν_0, the width Γ and the asymmetry q. In order to determine their values, we numerically convolved the Doppler and the Fano profiles, and varied the four parameters until a least squares fit to the experimental data was obtained.

A total of 26 transitions from $X\,^1\Sigma_g^+$ to $B''\,^1\Sigma_u^+$ ($v=2$), $D^1\Pi_u$ ($v=4$ in H_2, $v=5$ in D_2) and $D''\,^1\Pi_u$ ($v=0$) in H_2, HD, and D_2 were studied. Typical spectra are shown in Fig. 4. The observed lines are listed in Table I. The experimental uncertainty for the line centers was ± 0.2 cm^{-1}, a value limited by the current resolution of the wavemeter used.[19] In cases where Fano profiles were observed, the uncertainty of the predissociative width Γ was $\pm 10\%$, while that of the asymmetry parameter q was $\pm 25\%$. Finally, we note that, although the analysis described above used the description given by Fano, it may be possible to apply the multiquantum defect method[5] to dissociative amplitudes of this type.

IV. DISCUSSION

A. $B''(4p\sigma)\,^1\Sigma_u^+$ in H_2 and HD

The predissociative width and asymmetry of the B'' ($v=2$) levels vary significantly with J (Fig. 5). In the notation of Eqs. (2) and (3), $|\phi\rangle \approx |\xi\rangle = |B'', v=2, J\rangle$, $|\Psi\rangle = |B', E, J\rangle$, $|i\rangle = |X, v=0, J\pm 1\rangle$. The matrix element responsible for predissociation is $M = \langle\Psi(R)|\,H(R)\,|\xi(R)\rangle$, where R is the internuclear distance. In first approximation,

$$M \approx M_0 \langle\Psi(R)|\,\xi(R)\rangle\ , \tag{4}$$

where M_0 is a constant. The $B'-B''$ interaction

TABLE I. Measured absorption lines in hydrogen in the vicinity of 83 nm.

Molecule	Transition El. – Vibr.	Rot.	Line center (cm^{-1}) This work	Other works		Line shape This work	Other works
H_2	$B''-X$ (2,0)	$P(1)$	120 750.6	120 749.8[a]	120 750.9[b]	Fano: $\Gamma=0.80\pm0.10$ cm^{-1}, $q=15\pm5$	
H_2	$B''-X$ (2,0)	$P(2)$	120 563.3	120 563.0[a]	120 563.5[b]	Fano: $\Gamma=0.47\pm0.07$ cm^{-1}, $q=18\pm5$	
H_2	$B''-X$ (2,0)	$P(3)$	120 308.4	120 308.9[a]	120 308.8[b]	Doppler width	
H_2	$B''-X$ (2,0)	$R(2)$	120 804.2	120 802.0[a]	120 804.1[b]	Doppler width	
H_2	$B''-X$ (2,0)	$R(3)$	120 643.3	120 643.8[a]	120 643.9[b]	Doppler width	
H_2	$D-X$ (4,0)	$Q(2)$	120 801.3	120 802.0[a]	120 800.8[b]	Doppler width	
H_2	$D-X$ (4,0)	$Q(3)$	120 589.5	120 589.0[a]	120 589.7[b]	Doppler width	
H_2	$D''-X$ (0,0)	$Q(1)$	120 112.9	120 111.9[a]	120 113.1[b]	Doppler width	
H_2	$D''-X$ (0,0)	$R(0)$	120 241.3	120 240.6[a]	120 241.4[b]	Doppler width	
H_2	$D''-X$ (0,0)	$R(1)$	120 256.4	120 241.2[a]	120 256.9[b]	Doppler width	
HD	$B''-X$ (2,0)	$P(1)$	120 443.4	120 443.5[a]		Doppler width	
HD	$B''-X$ (2,0)	$R(0)$	120 570.3	120 570.0[a]		Doppler width	
HD	$B''-X$ (2,0)	$R(1)$	120 555.4	120 555.3[a]		Fano: $\Gamma=0.30\pm0.03$ cm^{-1}, $q=29\pm10$	
HD	$B''-X$ (2,0)	$R(2)$	120 489.3	120 488.6[a]		Fano: $\Gamma=0.27\pm0.03$ cm^{-1}, $q=43\pm15$	
HD	$B''-X$ (2,0)	$R(3)$	120 370.2	120 371.6[a]		Doppler width	
HD	$D''-X$ (0,0)	$Q(1)$	120 275.4	120 273.8[a]	120 276.1[c]	Doppler width	
D_2	$D-X$ (5,0)	$Q(1)$	120 527.9	120 527.3[a]		Doppler width	
D_2	$D-X$ (5,0)	$Q(2)$	120 451.9	120 452.0[a]		Doppler width	
D_2	$D-X$ (5,0)	$R(0)$	120 585.5	120 583.8[a]		Fano: $\Gamma=1.5\pm0.2$ cm^{-1}, $q=-22\pm4$	$\Gamma<2.3$ cm^{-1}[(d)]
D_2	$D-X$ (5,0)	$R(1)$	120 576.1	120 574.4[a]		Fano: $\Gamma=2.5\pm0.3$ cm^{-1}, $q=-7.5\pm1.5$	$\Gamma=3.6$ cm^{-1}[(d)]
D_2	$D-X$ (5,0)	$R(2)$	120 532.0	120 530.8[a]		Fano: $\Gamma=4.4\pm0.4$ cm^{-1}, $q=-4\pm1.0$	$\Gamma=7.6$ cm^{-1}[(d)]
D_2	$D''-X$ (0,0)	$Q(1)$	120 465.7	120 464.4[a]	120 466.6[e]	Doppler width	
D_2	$D''-X$ (0,0)	$Q(3)$	120 315.0	120 314.8[a]	120 315.7[e]	Doppler width	
D_2	$D''-X$ (0,0)	$R(0)$	120 529.5	120 528.7[a]	120 528.8[e]	Doppler width	
D_2	$D''-X$ (0,0)	$R(1)$	120 532.8	120 532.1[a]	120 532.3[e]	Doppler width	
D_2	$D''-X$ (0,0)	$R(3)$	120 454.3	120 454.0[a]	120 455.2[e]	Doppler width	

[a]Reference 15.
[b]Reference 28.
[c]Reference 29.
[d]Reference 11.
[e]Reference 30.

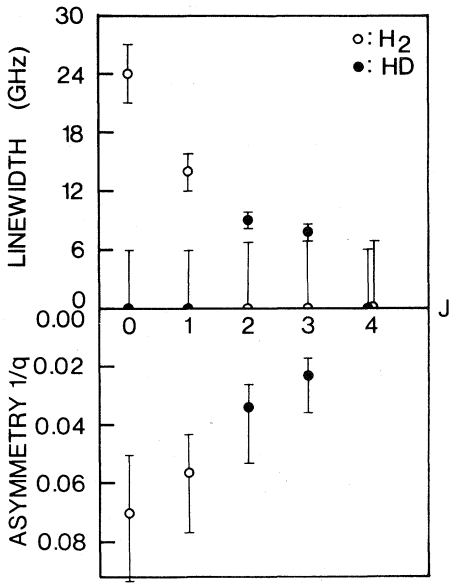

FIG. 5. The variation of predissociative width Γ and of asymmetry $1/q$, as a function of J in the B'' $(v=2)$ band of H_2 and HD. Only the asymmetry of states with $\Gamma \gtrsim 7$ GHz is shown.

is homogeneous, and therefore M_0 is independent of J. The matrix elements $\langle \xi | T | i \rangle$, $\langle \Psi | T | i \rangle$, both representing $^1\Sigma - {}^1\Sigma$ transitions, have the same J dependence. Therefore, the only source for the variations in Fig. 5 is the result of varying overlap integrals $\langle \Psi | \xi \rangle$ with changing J. From Eqs. (2) and (3)

$$[1/q(J)]^2 \propto \Gamma(J) \ . \tag{5}$$

As long as the predissociation is homogeneous Eq. (5) holds, even when approximation (4) fails. Equation (4) was, however, used in a semiquantitative fit of the H_2 data in Fig. 5. The fit showed that the Franck-Condon factor $|\langle \Psi | \xi \rangle|^2$ varies by amounts comparable to those observed experimentally. In this fit, the known potential curves[21] of the bound state (B'') and the continuum state (B') were approximated by a Morse potential,[22]

$$U(R) = U_0 + A(e^{-2\alpha(R-R_0)} - 2e^{-\alpha(R-R_0)}) \tag{6}$$

and by a linear slope,[22]

$$V(R) = a + bR, \tag{7}$$

respectively. Variation of the parameter a [Eq. (7)] corresponds to a change in the distance between the two curves, a procedure which simulates a variation in the rotational quantum number J. Numerical integration of the resulting Morse (for B'') and Airy (for B') functions showed that the fast oscillations of the Airy function can produce substantial changes (by a factor of two to three) in the value of $|\langle \Psi | \xi \rangle|^2$ on a relatively small energy scale (~ 100 cm^{-1}). The rotational constant of B'' $(v=2)$ is[23] $B_e \approx 27$ cm^{-1}, so that the energy spanned by $J=0$ to $J=4$, (Fig. 5) is ~ 540 cm^{-1}.

While the above calculations are in good qualitative agreement with our experimental results, the approximations of Eqs. (4), (6), and (7) do not enable a more accurate quantitative comparison.

Similar calculations can be performed for HD. However, since the center of mass and the center of charge do not coincide, the evaluation of the coupling matrix element M is more complicated. Nevertheless, under the approximation of Eq. (4), qualitatively similar results were obtained for HD and H_2. It should also be noted that, within experimental uncertainty, Eq. (5) is fulfilled for H_2 as well as for HD.

The absolute cross section for the $B'' \leftarrow X$ transition was determined as outlined in Sec. II above. We found that the peak cross section, not including the rotational Hönl-London factors,[16] was $\sigma_{pk} = (7.2 \pm 0.7) \times 10^{-16}$ cm^2. With an average line width of 1.1 cm^{-1}, the matrix element of the $B'' \leftarrow X(2,0)$ transition is

$$|(M^{el})(M^{vib})| = (0.047 \pm 0.005) \text{ a.u.} \tag{8}$$

In Eq. (8), M^{vib} is the square root of the Franck-Condon factor. Assuming similarity in shapes of the B' and B'' potential curves, $|M^{vib}| \approx 0.31 \pm 0.03$.[24] Hence, $(M^{el})^2 = (0.022 \pm 0.003)$ a.u., which corresponds to (0.38 ± 0.05) D.

B. $D(3p\pi)\,{}^1\Pi_u$ and $D''(5p\pi)\,{}^1\Pi_u$ in H_2, HD

The observed Q lines of $D \leftarrow X$ $(4,0)$ in H_2, as well as the P- and R-branch lines of $D'' \leftarrow X(0,0)$ in H_2 and HD exhibited symmetric, Gaussian profiles (Table I). From this observation we conclude that the predissociative widths of the upper states in these transitions are less than ~ 0.08 cm^{-1}. This fact is in conformance with the considerations mentioned above, i.e., that the predissociation of ${}^1\Pi_u^-$ states and the accidental predissociation of $(np\pi)\,{}^1\Pi_u^+$ $(n \geq 4)$ states are weak.

C. $D(3p\pi)\,{}^1\Pi_u$ and $D''(5p\pi)\,{}^1\Pi_u$ in D_2

Although the electronic potential curves are only slightly influenced by isotopic substitution of the nuclei, the vibrational and rotational constants are significantly affected.[16] Thus, the spacing between ro-vibrational states belonging to different electronic configurations may be strongly isotope-de-

pendent. In particular, accidental resonances, which may cause irregularities in predissociative rates, may occur in one isotopic derivative of hydrogen and not in others. This fact enables exaggerated isotopic effects to arise. Such is the case in D_2, where the D ($v=5$) and D'' ($v=0$) rotational states are accidentally close enough to perturb each other significantly. This perturbation is homogeneous ($\Delta\Lambda=0$), thereby rendering it independent of J. Changes in Franck-Condon factors are expected to be much less pronounced than in the $B'-B''$ interaction, because both D ($v=5$) and D'' ($v=0$) are bound states with relatively slow oscillations in their wave functions. On the other hand, the predissociative $D-B'$ interaction is heterogeneous, and the coupling matrix element is proportional to $[J(J+1)]^{1/2}$. In the notation of Eqs. (2) and (3), for R-branch transitions: $|i\rangle=|X,\ v=0,\ J-1\rangle$, $|\Psi\rangle=|B',\ E\ J\rangle$. If there is no $D-D''$ coupling, as for instance is the case in H_2, then $|\phi\rangle\approx|\xi\rangle=|D,\ v=5,\ J\rangle$ and[3]

$$\Gamma(J)\propto J(J+1)\ , \tag{9}$$

$$1/q\propto J. \tag{10}$$

As is evident from Table I, $\Gamma(J)$ increases more slowly than predicted by Eq. (9), whereas $1/q$ increases somewhat faster than J [Eq. (10)]. This anomaly cannot be explained by variations in the $B'-D$ overlap integral, because then q and Γ would have to satisfy the relation

$$\left(\frac{1}{q(J)}\right)^2\propto\frac{J}{J+1}\,\Gamma(J)\ . \tag{11}$$

Relationship (11) is clearly *not* satisfied by our experimental data.

The deviation of $\Gamma(J)$ and $q(J)$ from their expected behavior [Eqs. (9) and (10)] is, however, explained by the mixing of the D and D'' states. On the basis of angular momentum conservation,[16] only states with equal J can perturb each other. In our case, the separation between pairs of states with equal J decreases with increasing J. As a result, the D states acquire an increasingly larger D'' character as J increases. The D'' state has a very small predissociative width (Table I), and, therefore, the increasingly larger amount of D'' mixed into D retards the quadratic behavior of $\Gamma(J)$, Eq. (9). The asymmetry $1/q$ can either increase or decrease as a result of the mixing, depending on the relative signs of the $D-X$ and $D''-X$ matrix elements, as noted below.

An exact treatment, which would yield a quantitative fit to the experimental data, must include all the pertinent interactions: $B'(3p\sigma)\,^1\Sigma_u^+ - D(3p\pi)\,^1\Pi_u$ (heterogeneous), $(5p\sigma)\,^1\Sigma_u^+ - D''(5p\pi)\,^1\Pi_u$ (heterogeneous), $B'(3p\sigma)\,^1\Sigma_u^+ - 5p\sigma\,^1\Sigma_u^+$ (homogeneous), and $D(3p\pi)\,^1\Pi_u - D''(5p\pi)\,^1\Pi_u$ (homogeneous). A simpler model can, however, be constructed, especially at the lower J values (large separation between interacting states). In this approximation the $D-D''$ perturbation is treated independently of the other interactions, and is superimposed on them. The mixed state is[16]

$$|\eta(J)\rangle=C_D(J)|D,\ v=5,\ J\rangle-C_{D''}(J)|D'',\ v=0,\ J\rangle\ , \tag{12}$$

where $C_D(J)$ and $C_{D''}(J)$ are positive, and are determined by the term values and the coupling matrix element. Also,

$$|C_D(J)|^2+|C_{D''}(J)|^2=1\ , \tag{13}$$

and the state $|\xi\rangle$ in Eqs. (2) and (3) should now be replaced by the mixed state $|\eta\rangle$. Since $\langle D''|H|B'\rangle\approx 0$, Eqs. (9) and (10) are modified to

$$\Gamma(J)\propto|C_D(J)|^2J(J+1)\ , \tag{14}$$

$$\frac{1}{q}\propto\frac{C_D(J)}{C_D(J)-(M_{D''-X(0,0)}/M_{D-X(5,0)})C_{D''}(J)}\,J\ . \tag{15}$$

In Eq. (15), the M's are the electronic-vibrational dipole moment matrix elements of the indicated transitions. Using Eq. (13), Eq. (15), can be written as

$$\frac{1}{q}\propto\frac{J}{1-(M_{D''-X(0,0)}/M_{D-X(5,0)})[1/|C_D(J)|^2-1]^{1/2}}\ . \tag{16}$$

It is now evident, that the asymmetry $|1/q|$ can increase or decrease as a result of $D-D''$ mixing, depending on the relative signs of $M_{D-X(5,0)}$ and $M_{D''-X(0,0)}$. If there were a change in sign from D ($v=5$) to D'' ($v=0$), the absorption cross section or the Franck-Condon factors would exhibit a minimum in the transition from one state to the other. No such minimum exists,[25,26] which leads to the conclusion that $r\equiv M_{D''-X(0,0)}/M_{D-X(5,0)}>0$. Referring to Eq. (16), $|1/q(J)|$ increases more rapidly than J, in qualitative agreement with the experimental data. Furthermore, good quantitative agreement exists between the behavior of $\Gamma(J)$, Eq. (14), that of $1/q(J)$, Eq. (16), and our experimental data, as detailed below.

From Eq. (14), $f(J)\equiv\Gamma(J)/[J(J+1)]\propto|C_D(J)|^2$. Experimentally (Table I), $f(1)=2.0\,f(3)$. Since $0.5\leq|C_D(J)|^2\leq 1$, the experimental data uniquely

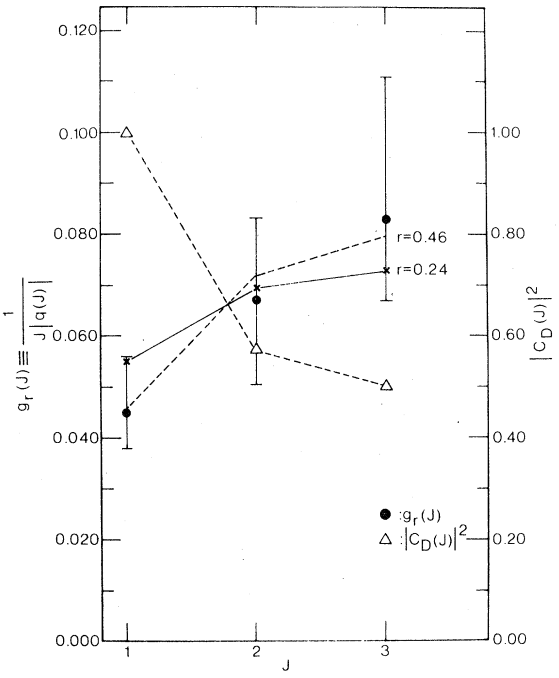

FIG. 6. The mixing coefficient $|C_D(J)|^2$ and the function $g_r(J)$ (see text) of the D $(v=5)$ band in D_2. The solid line is the best fit of $g_r(J)$ to the experimental points with $r=0.24$. The broken line is the best fit, when r was also allowed to vary; in this case the best value of r was $r=0.46$.

determine $|C_D(J)|^2$: $|C_D(1)|^2=1.0$, $|C_D(2)|^2=0.57$, $|C_D(3)|^2=0.50$. These values, found from $\Gamma(J)$, determine $1/q(J)$, if $r=M_{D''-X\,(0,0)}/M_{D-X\,(5,0)}$ is known [Eq. (16)]. The latter quantity was approximated as follows. The vibrational part is[26] $M^{\rm vib}_{D''-X\,(0,0)}/M^{\rm vib}_{D-X\,(5,0)} \approx M^{\rm vib}_{D-X\,(0,0)}/M^{\rm vib}_{D-X\,(5,0)}=0.58$. The electronic part is approximately that of the hydrogen atom[27]: $(M^{\rm el}_{D''-X}/M^{\rm el}_{D-X})_{D_2} \approx (M_{1s-5p}/M_{1s-3p})_H=0.41$. Hence, $r\approx 0.24$, and the asymmetry $1/q$ is now determined. Figure 6 shows the excellent agreement between the predicted [Eq. (16)] and measured values of $g_r(J)\equiv 1/[J|q(J)|]$.

The above analysis shows that the measured values of $\Gamma(J)$ and of $q(J)$ for $J=1$, 2, 3 of D $(v=5)$ in D_2 are consistent with a $D-D''$ perturbation and it also determines the coefficients of mixing $|C_D(J)|^2$. The next step, that of independently determining $|C_D(J)|^2$ from the known term values, is complicated by the existence of the other interactions mentioned above. At the present time, this more involved analysis has not been completed.

V. CONCLUSION

A new, high spectral brightness source at 83 nm has been used to conduct spectroscopic studies of certain Rydberg states in molecular hydrogen with 0.2-cm^{-1} resolution. Numerical analysis based on the theory developed by Fano identified the existence and extent of certain line shape-determining factors in predissociated states: overlap integrals can influence the predissociative linewidths to vary by factors of two to three over less than a 0.05-eV energy span. Accidental isotope-selective near-resonances can mix a weakly predissociated state with a strongly predissociated one, causing substantial changes in both the linewidth and the line shape.

ACKNOWLEDGMENTS

We acknowledge the assistance of T. Srinivasan and M. Wilson with data acquisition and analysis. The technical help of K. Skala and S. Vendetta is greatly appreciated. This work was supported by the National Science Foundation under Grant No. PHY78-27610, the Department of Energy under Contract Nos. DE-AC02-80-ET33065. A000 and DE-AD2-79-ER-10350, the Air Force Office of Scientific Research under Grant No. AFOSR-79-0130, and the Office of Naval Research.

*Present address: Amoco Research Center, P.O. Box 400, Naperville, Illinois 60540.
†Present address: Bell Laboratories, Holmdel, New Jersey 07733.

[1] P. Borrell, P. M. Guyon, and M. Glass-Maujean, J. Chem. Phys. 66, 818 (1977).
[2] M. Glass-Maujean, J. Breton, and P. M. Guyon, Phys. Rev. Lett. 40, 181 (1978).
[3] M. Glass-Maujean, J. Breton, and P. M. Guyon, Chem. Phys. Lett. 63, 591 (1979).
[4] G. Herzberg and Ch. Jungen, J. Mol. Spectrosc. 41, 425 (1972).
[5] Ch. Jungen and O. Atabek, J. Chem. Phys. 66, 5584 (1977).
[6] O. Gallais, Mol. Phys. 25, 949 (1973).
[7] P. S. Julienne, J. Mol. Spectrosc. 48, 508 (1973).
[8] W. Kołos, J. Mol. Spectrosc. 62, 429 (1976).
[9] D. J. Kligler and C. K. Rhodes, Phys. Rev. Lett. 40, 309 (1978).
[10] P. M. Dehmer and W. A. Chupka, Chem. Phys. Lett. 70, 127 (1980).
[11] F. J. Comes and G. Schumpe, Z. Naturforsch. 26a, 538 (1971).
[12] J. Breton, P. M. Guyon, and M. Glass-Maujean, Phys. Rev. A 21, 1909 (1980).
[13] M. Rothschild, H. Egger, R. T. Hawkins, H. Pummer, and C. K. Rhodes, Chem. Phys. Lett. 72, 404 (1980).
[14] H. Egger, R. T. Hawkins, J. Bokor, H. Pummer,

M. Rothschild, and C. K. Rhodes, Opt. Lett. 5, 282 (1980).
[15]A. Monfils, J. Mol. Spectrosc. 15, 265 (1965).
[16]G. Herzberg, *Spectra of Diatomic Molecules* (Van Nostrand, New York, 1950).
[17]P. M. Guyon, J. Breton, and M. Glass-Maujean, Chem. Phys. Lett. 68, 314 (1979).
[18]M. Glass-Maujean, Chem. Phys. Lett. 68, 320 (1979).
[19]R. T. Hawkins, H. Egger, J. Bokor, and C. K. Rhodes, Appl. Phys. Lett. 36, 391 (1980).
[20]U. Fano, Phys. Rev. 124, 1866 (1961).
[21]T. E. Sharp, At. Data 2, 119 (1971).
[22]L. D. Landau and E. M. Lifschitz, *Quantum Mechanics* (Addison-Wesley, Reading, Massachussetts, 1965).
[23]K. P. Huber and G. Herzberg, *Constants of Diatomic Molecules* (Van Nostrand, New York, 1979).
[24]R. J. Spindler, J. Quant. Spectrosc. Radiat. Transfer 9, 1041 (1969).
[25]K. J. Miller and M. Krauss, J. Chem. Phys. 47, 3754 (1967).
[26]M. Halmann and I. Laulicht, Astrophs. J. Suppl. Ser. 12, No. 110, p. 307 (1966).
[27]H. A. Bethe and E. E. Salpeter, *Quantum Mechanics of One- and Two-Electron Atoms* (Plenum, New York, 1977).
[28]S. Takezawa, J. Chem.Phys. 52, 2575 (1970).
[29]S. Takezawa and Y. Tanaka, J. Chem. Phys. 56, 6125 (1972).
[30]S. Takezawa and Y. Tanaka, J. Mol. Spectrosc. 54, 379 (1975).